Experimental Mechanics (2006) 46: 725–733
DOI 10.1007/s11340-006-9659-3

Mechanical Properties of Microcapsules Used in a Self-Healing Polymer

M.W. Keller · N.R. Sottos

Received: 16 November 2005 / Accepted: 28 June 2006 / Published online: 23 November 2006

Abstract The elastic modulus and failure behavior of poly(urea-formaldehyde) shelled microcapsules were determined through single-capsule compression tests. Capsules were tested both dry and immersed in a fluid isotonic with the encapsulent. The testing of capsules immersed in a fluid had little influence on mechanical behavior in the elastic regime. Elastic modulus of the capsule shell wall was extracted by comparison with a shell theory model for the compression of a fluid filled microcapsule. Average capsule shell wall modulus was 3.7 GPa, regardless of whether the capsule was tested immersed or dry. Microcapsule diameter was found to have a significant effect on failure strength, with smaller capsules sustaining higher loads before failure. Capsule size had no effect on the modulus value determined from comparison with theory.

Keywords Self-healing composite · Microcapsule · Compression · Urea-formaldehyde · Modulus · Strength

Introduction

Microcapsules containing liquid healing agent are a critical component of self-healing polymers [1, 2]. Healing is accomplished by incorporating the microencapsulated healing agent and a catalyst within an epoxy matrix. An approaching crack ruptures embedded microcapsules, releasing healing agent into the crack plane through capillary action. Polymerization of the healing agent is initiated by contact with the embedded chemical catalyst, bonding the crack faces. The rupture of microcapsules is the mechanical trigger to the healing process and without it, no healing occurs. This system has proven to be highly effective at healing cracks in both quasi-static [1] and fatigue [3–6] loading.

An optimal combination of microcapsule and matrix properties is necessary to ensure mechanical triggering when the material is damaged; if the shell wall is too thick the microcapsule will not rupture readily, preventing the release of healing agent. On the other hand, if the shell wall is too thin, the capsules not only are fragile, but also allow diffusion of the healing agent into the matrix. Other key parameters for efficient healing agent delivery are the elastic stiffness, the failure strength of the capsules, and the fill content, which is the percentage of the capsule core volume occupied by the encapsulated fluid.

Because the variable set describing the behavior of microcapsules in a matrix is large, micromechanical modeling can be used to investigate the interaction of a crack with a microcapsule. In previous work, Eshelby–Mura equivalent inclusion method was chosen to perform the modeling of the crack-capsule interaction [1]. Model predictions reveal that that the capsule-to-matrix stiffness ratio influences the crack propagation path in close proximity to the capsule. A capsule with a higher elastic modulus than the surrounding matrix creates a stress field that tends to deflect the crack away from the microcapsule. Conversely, a more compliant

M.W. Keller (✉, SEM member) · N.R. Sottos (SEM member)
Department of Theoretical and Applied Mechanics and Beckman Institute for Advanced Science and Technology, University of Illinois at Urbana-Champaign, Urbana, IL 61801, USA
e-mail: mwkeller@uiuc.edu

shell wall material produces a stress field that attracts the crack toward the microcapsule, facilitating capsule rupture.

In addition to providing storage of the healing monomer, Brown et al. [7] demonstrated that the inclusion of microcapsules can toughen a polymer matrix by 127%, when compared to the fracture toughness of the unfilled matrix. Previous studies of microcapsule toughening included only the effect of average capsule diameter and volume faction. The additional influences of shell wall thickness, capsule processing, and fill content on toughening in a polymer matrix were examined in more recent work [8]. While all three of these parameters significantly impacted the efficiency of microcapsule toughening, it was difficult to elucidate the relationship between physical properties of the microcapsule and the fracture performance of the polymer composite. The goal of the present work is to characterize the mechanical properties of the microcapsule system currently used in self-healing composites.

Several methods for characterizing capsules have appeared in the literature, most of which were developed for probing the mechanical response of biological cells. Mitchison and Swan [9] introduced a micropipette aspiration test for probing the mechanical response of biological cells. A micropipette was placed in contact with the cell and a vacuum was applied, drawing the cell wall into the micropipette. The cell wall deflection was measured and related to the mechanical stiffness of the wall material. The micropipette aspiration technique has also been applied to determine microcapsule shell wall elastic modulus [10]. Cole used a simple compression test to characterize the stiffness of sea urchin eggs [11]. A single egg was placed between two platens and then compressed. In addition to characterizing biological cells, this experimental technique has been applied to microcapsule systems [12–14]. Lulevich and coworkers have used modified atomic force microscopy (AFM) cantilevers to compress small, about 5 microns in diameter, microcapsules [15]. Compression experiments using an AFM indenter have also been combined with Reflection Interference Contrast Microscopy (RICM) to determine capsule shape [16]. In RICM, the sample is illuminated in reflection and the reflected light produces interference fringes that can be used to ascertain the microcapsule shape. Beyond capsule compression and micropipette aspiration, a capsule indentation technique has been developed by Gordon et al. [17] and Hsu et al. [18]. This technique uses calibrated micropipettes to indent the surface of a microcapsule, the resulting indentation shape can then be compared with finite element predictions to back out capsule shell wall properties.

In the current work, the single-capsule compression experiment is adopted for the characterization of a range of microcapsules and the resulting load-displacement data compared with a shell theory model to determine the elastic properties of the shell wall. The compression experiment was chosen primarily because of its simplicity. Compression testing requires little specialized equipment and can be used to test a wide variety of capsules in different environments. For example, this test can be used to characterize dry capsules or capsules that are immersed in a fluid. Compression testing also measures two capsule properties in a single test, shell wall modulus, on comparison with a model, and capsule failure strength. The modeling of this test is not as straight forward as the pipette aspiration technique mentioned above, but it does not require finite element analysis or other specialized modeling techniques.

Experimental Procedure

Capsule Manufacture

The capsules examined in this study had a poly(urea-formaldehyde)(UF) shell wall and were filled with dicyclopentadiene (DCPD) liquid monomer. They were identical to those used for the self-healing system in [1] and were manufactured by an in-situ microencapsulation method. In-situ microencapsulation proceeds in two concurrent steps. First a UF prepolymer is formed in an aqueous bath containing an emulsified, water-immiscible encapsulent fluid [19]. The UF polymerizes around an individual DCPD droplet in the emulsion, forming the shell wall of an individual microcapsule. Capsule diameter is determined by the droplet size of the emulsion. A schematic of the procedure for manufacturing UF capsules is presented in Fig. 1. The average diameters for each capsule group tested were $213\pm12\ \mu$m, $187\pm15\ \mu$m, and $65\pm7\ \mu$m.

A representative scanning electron microscopy (SEM) micrograph of the surface morphology of a UF capsule is shown in Fig. 2. In addition to allowing investigation of surface morphology, SEM enabled measurement of the shell wall thickness of an individual capsule. These microcapsules possessed a highly uniform shell wall thickness, 175 ± 33 nm, independent of capsule diameter.

Experimental Setup

The capsule compression apparatus, shown in Fig. 3, was adapted from the one described by Liu and coworkers [12]. Displacement was applied at a rate of

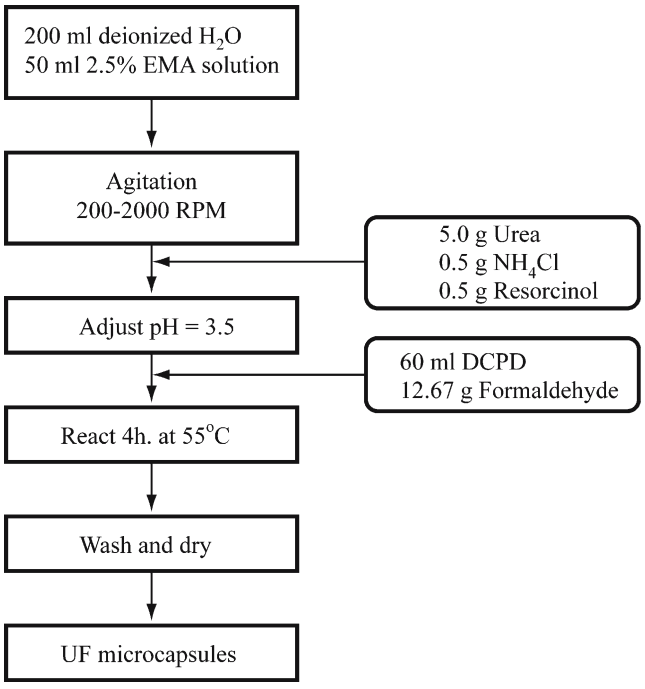

Fig. 1. Encapsulation procedure for UF capsules [19]

5 μm/s for the 187 and 213 μm capsule size ranges and 2.5 μm/s for the 65 μm size range using a stepper actuator (Physik Insturmente M-230S) controlled via a computer interface and accurate to 50 nm. Load data were acquired from a 10 g load cell (Transducer Techniques GSO-10) via a DAQ card (PCI-MIO-16E-4) and associated software from National Instruments giving a combined sensor system accuracy of ±100 nN. Images of the capsule during the compression cycle were captured through a stereo microscope (Nikon SMZ-2T) by a monochrome CCD Camera (Qimaging Retiga). The entire system was mounted on a vibration isolation table.

For a dry microcapsule test, capsules were drawn into a pipette, which enabled release of a single capsule onto the compression platen. An image of the microcapsule was taken prior to compression to determine the initial capsule diameter. An initial separation between the capsule and punch allowed the stepper to achieve steady-state velocity after motion was initiated. The test program was started after positioning the punch above the capsule and terminated after failure was observed.

Immersion tests were conducted using a modification of the apparatus presented in Fig. 3. A schematic of the modified compression setup and the immersion test cell are shown in Fig. 4. Capsules tested in the immersion setup were dispersed in a bath of DCPD and allowed to equilibrate for at least 24 h. While the microcapsule wall is assumed to be impermeable on short time scales, there will be some diffusive mobility across the membrane on long time scales. Then a single capsule was removed from solution by pipetting and placed into the compression cell. Fluid was added to the cell cavity to ensure that the entire capsule was submerged. Testing then proceeded as described for the dry test.

Compression Test Results

Figure 5 shows representative load-displacement data for an immersed capsule, 213 μm in diameter, tested in compression. Dimensionless displacement is defined by the displacement, δ, divided by the initial capsule diameter, D. Capsules tested while immersed in the encapsulent fluid were imaged by backlighting. In Fig. 5 the images numbered one through four show the capsule during representative sections of the loading sequence. In these images, the solid white line indicates the bottom of the compression platen and the dark

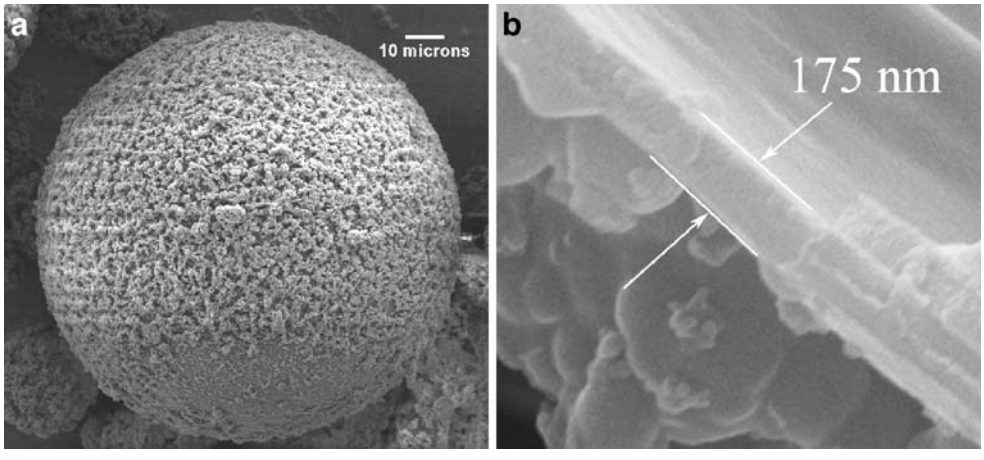

Fig. 2. Electron micrographs of a UF DCPD filled microcapsule: (**a**) surface morphology; (**b**) cross-section of the shell wall

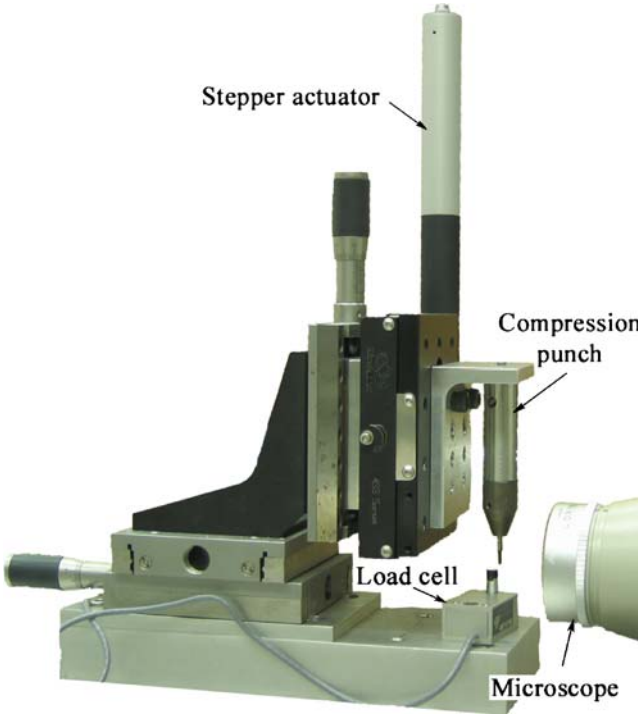

Fig. 3. Photograph of experimental setup

region is the compression punch. Image 1 shows the capsule prior to contact with the compression platen. Image 2 is the capsule near the 15% dimensionless displacement point. At approximately this displacement, other researchers have observed a 'yield' in the load-displacement response. This yield is characterized by a change in concavity of the load-displacement curve [13]. Repeated compressions of a single capsule to 20% dimensionless displacement show a reduction in the peak load attained for each sucessive compression. This load reduction would tend to indicate the presence of progressive damage. Image 3 captures the capsule near the failure event, which is indicated by the load peak, and image 4 is the capsule after failure.

From Fig. 5 two key observations of compressive capsule shell wall behavior are evident: the capsule shell wall does not buckle during compression and, the capsule remains effectively intact after failure. The absence of buckling indicates that the yield point is due to localized damage, such as microcracking or shear yielding, of the shell wall material. The failure event was also studied with dry compression tests utilizing capsules filled with dyed DCPD. In the dye tests, the encapsulent fluid was dyed using an oil-soluble dye. The compression test was then imaged optically with a color camera to attempt to detect the associated color change if dyed DCPD was leaked onto the surface of the capsule. These tests were able to capture the gross capsule failure event and failure was observed to proceed from the edge of the contact zone where the radius of curvature is the highest. This failure is not a dynamic event such as a burst, but a leaking of encapsulent fluid from a shell wall failure. The encapsulent leakage proceeds quickly, coating the surface of the capsule in a few seconds.

Figure 6 is a comparison of compression results for dry and immersed capsules of similar diameters. The load-displacement responses of these tests are quite similar in the elastic region of the test (dimensionless displacement less than 15%). At about 20% dimensionless displacement, however, the capsule response changes. The dry capsules generally sustain more load prior to failure than the immersed capsules.

Capsules from batches with average diameters of 187 ± 15 μm and 65 ± 7 μm were tested in dry compression to determine the effect of capsule size. Figure 7 shows representative load-displacement responses for each of the capsule diameters. Two size effects can be noted: smaller capsules are less stiff as a system, in the sense that they sustain less load for a given dimensionless displacement, and the maximum load at failure is highly diameter dependent. The dependence of failure strength on capsule diameter has been observed previously [13]. Table 1 shows the average failure force and failure strength of the microcapsule types tested. The failure strength is calculated as the failure force normalized by capsule cross-sectional area. The strength data indicate that during dry compression, smaller capsules are harder to failure than their larger counterparts.

Comparison with Theory

Model Development

The elastic modulus of the capsule shell wall material is extracted through comparison with an analytical

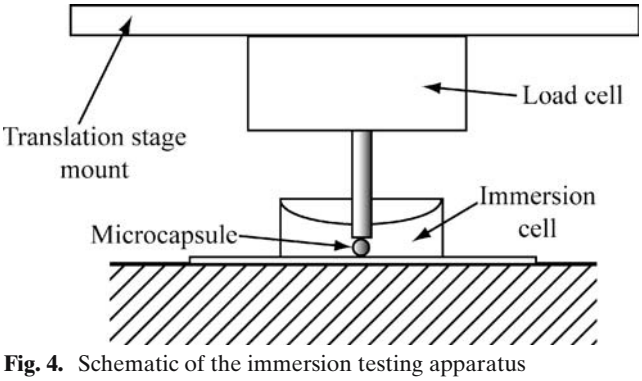

Fig. 4. Schematic of the immersion testing apparatus

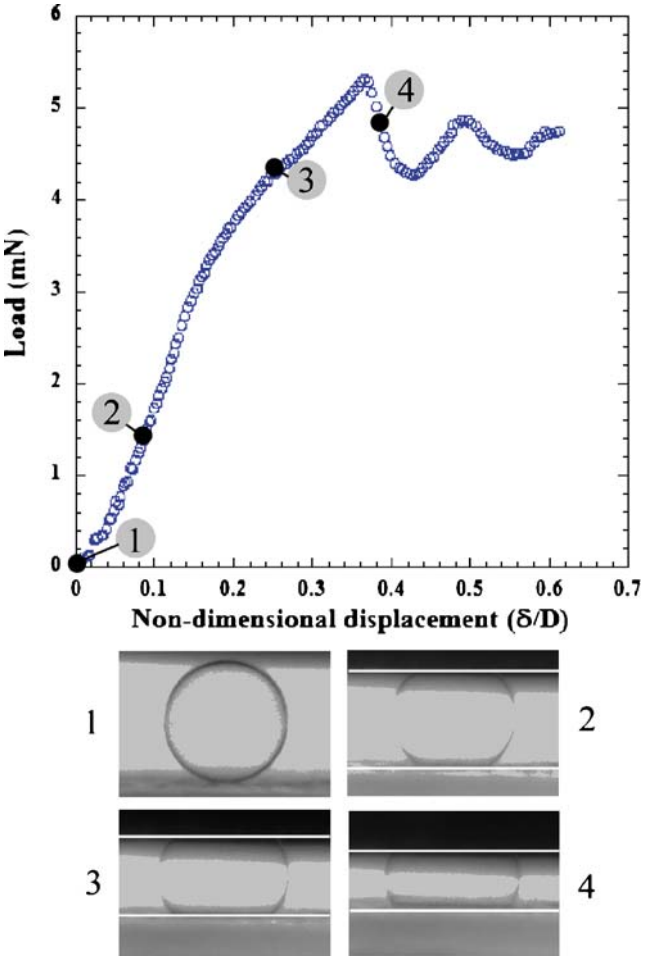

Fig. 5. Images of a 213 μm diameter capsule during an immersed compression test

membrane theory model. The model is based on the theory initially developed by Feng and Yang [20] for an inflated spherical membrane and then later extended to fluid-filled shells by Lardner and Pujara [21]. The current work follows the analysis for fluid-filled shells as presented in [22] that assumes an isotropic, linear elastic constitutive relationship for the shell wall material. Additionally, as this is a membrane shell model, the bending resistance of the capsule shell wall is neglected. The capsules are observed to deflate into a crumpled state after the encapsulating fluid is removed by evaporation, which implies that this assumption is valid. If the capsule had remained spherical upon removal of the encapsulated fluid this bending resistance should not be neglected. From Table 1 the shell wall thickness to diameter ratios, t/D, are also very small, validating again the assumption that the bending resistance of the microcapsules is negligible. A summary of the model is presented below along with comparisons with the current compression data.

The compression of a microcapsule is shown schematically in Fig. 8, where the solid line is the uncompressed profile and the dashed line represents the compressed geometry.

Two systems of ordinary differential equations (ODEs) describe the deformation of a microcapsule one for the contact region one system for the non-contact region. The contact region, the flat portion of the dashed profile, is constrained in one dimension by the compression punch. The non-contact region, which comprises the rest of the capsule shell, is unconstrained and can deform freely.

The system of ODEs for the contact region are

$$\lambda_1' = -\frac{\lambda_1}{\lambda_2 \sin\psi}\frac{f_3}{f_1} - \frac{\lambda_1 - \lambda_2\cos\psi}{\sin\psi}\frac{f_2}{f_1}, \tag{1}$$

$$\lambda_2' = \frac{\lambda_1 - \lambda_2\cos\psi}{\sin\psi}, \tag{2}$$

where ψ is the angular coordinate of the compressed capsule, λ_1 and λ_2 are the principal stretch ratios with the 1 denoting the meridional orientation and the 2 circumferential direction, and f_1, f_2, and f_3 are

$$f_1 = \frac{\partial T_1}{\partial \lambda_1}, \tag{3}$$

$$f_2 = \frac{\partial T_2}{\partial \lambda_2}, \tag{4}$$

$$f_3 = T_1 - T_2, \tag{5}$$

where T_1 and T_2 are the membrane tensions.

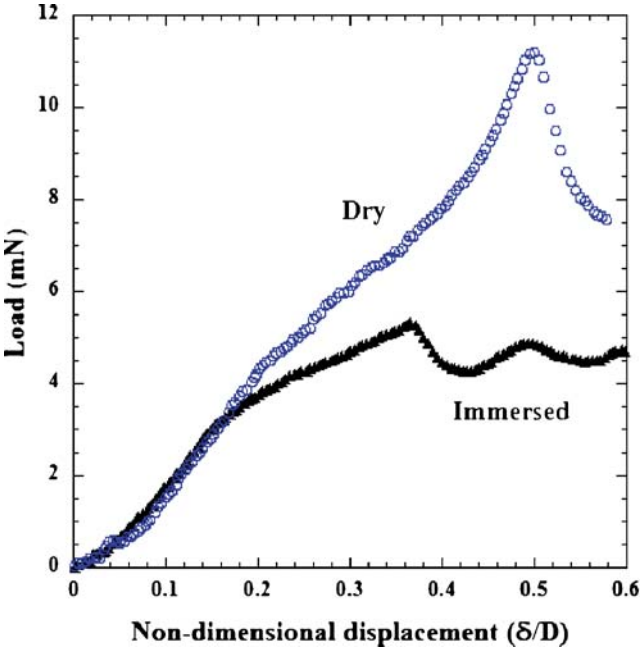

Fig. 6. Comparison of dry and immersed tests on capsules of similar diameter (222 μm)

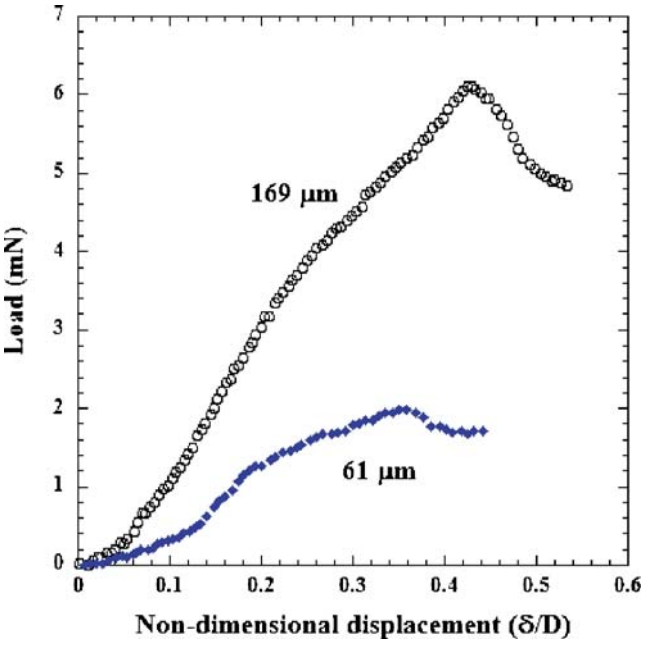

Fig. 7. Comparison of load-displacement responses for a 169 μm diameter microcapsule and a 61 μm diameter microcapsule tested in dry compression

The ODEs for the non-contact region are

$$\lambda_1' = \frac{\delta\cos\psi - \omega\sin\psi}{\sin^2\psi}\frac{f_2}{f_1} - \frac{\omega}{\delta}\frac{f_3}{f_1}, \tag{6}$$

$$\delta' = \omega \tag{7}$$

$$\omega' = \frac{\lambda_1'\omega}{\lambda_1} + \frac{\lambda_1^2 - \omega^2}{\delta}\frac{T_2}{T_1} - \frac{\lambda_1(\lambda_1^2 - \omega^2)^{1/2}Pr_0}{T_1}, \tag{8}$$

where

$$\delta = \lambda_2\sin\psi. \tag{9}$$

An isotropic, linear elastic constitutive relationship was assumed for the current microcapsule systems and was derived following [22]. The linear-elastic strain energy formula is

$$W = \frac{Eh_0}{2\left(1+\nu^2\right)}\{(\lambda_1-1)^2 + (\lambda_2-1)^2 + 2\nu(\lambda_1-1)(\lambda_2-1)\} \tag{10}$$

from [23]. The wall tensions T_i are related to the strain energy by

$$T_i = \frac{1}{\lambda_1\lambda_2}\frac{\partial W}{\partial\lambda_i}(\lambda_i)^2. \tag{11}$$

Equation (10) with equation (11) yields

$$T_1 = \frac{Eh_0}{(1-\nu^2)}\frac{\lambda_1}{\lambda_2}\{(\lambda_1-1) + \nu(\lambda_2-1)\}, \tag{12}$$

$$T_2 = \frac{Eh_0}{(1-\nu^2)}\frac{\lambda_2}{\lambda_1}\{(\lambda_2-1) + \nu(\lambda_1-1)\} \tag{13}$$

for the shell wall tensions. The boundary conditions for this problem are

$$\begin{aligned}
&\psi = 0 : \lambda_1 = \lambda_2 = \lambda_0,\\
&\psi = \Gamma : \lambda_{1,\text{contact}} = \lambda_{1,\text{non-contact}},\\
&\psi = \Gamma : \lambda_{2,\text{contact}} = \lambda_{2,\text{non-contact}},\\
&\psi = \Gamma : \eta' = 0,\\
&\psi = \frac{\pi}{2} : \delta' = 0.
\end{aligned} \tag{14}$$

The above system of ODEs were solved using the numerical scheme outlined in [20], where the independent variable is the angular coordinate, ψ, in the undeformed reference frame. Numerical solutions were performed with a Runge–Kutta solver provided by Matlab (The MathWorks Inc.). Input to this program consisted of the measured capsule diameter and the average wall thickness. The Poisson's ratio ν was assumed to be 1/3, a value consistent with other formaldehyde-based polymers. Since the problem is time independent, the load-displacement plots were generated by solving the equilibrium problem of the capsule for a given contact radius and determining the corresponding cross-head displacement.

Table 1 Average Young's modulus and failure behavior of tested microcapsules

Average diameter (μm ± Std. dev.)	t/D	E (GPa ± Std. dev.)	Average failure force (mN ± Std. dev.)	Normalized failure strength (MPa ± Std. dev.)
187±15, dry	0.001	3.6 ± 0.4	6.5 ± 1.6	0.24 ± 0.04
213±12, immersed	0.001	3.9 ± 0.7	4.9 ± 0.5	0.14 ± 0.02
65±7, dry	0.004	3.7 ± 0.5	2.7 ± 0.7	0.8 ± 0.3

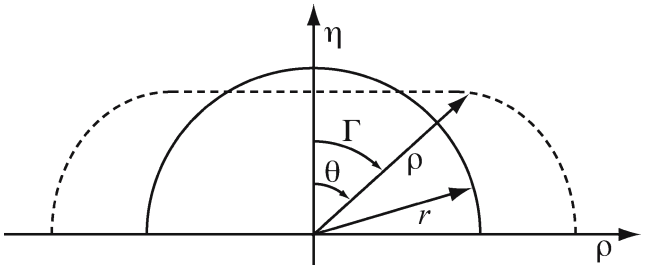

Fig. 8. Schematic of the microcapsule compression problem. The solid line is the uncompressed microcapsule and the dashed line is the compressed microcapsule, after the figure in [12]

A sensitivity study was undertaken to investigate the influence of Poisson's ratio choice on the calculated load-displacement response. Figure 9 shows the non-dimensional force ($F = P/Eh_0r_0$)–dimensionless displacement response for different values of the Poisson's ratio. The model exhibits little sensitivity to Poisson's ratio, and the results shown in Fig. 9 are independent of capsule diameter or shell wall thickness. The sensitivity to shell wall thickness variation was also investigated numerically. Figure 9 contains predicted load-displacement curves for a hypothetical capsule with a diameter of 180 μm and a shell wall modulus of 3.6 GPa. The family of curves are the calculated load-displacement responses if the shell wall is assumed to be the average thickness, the upper thickness limit, and the lower thickness limit measured by SEM on a microcapsule batch. These numerical studies indicate that variation in the shell wall thickness alters the predicted modulus value by the same percentage as the thickness variation. That is, if the shell wall is assumed to be 20% thicker than the actual value, the modulus will be under-predicted by 20%. Additionally, the encapsulated volume is assumed constant, as in previous studies [12, 21]. The constant volume assumption disallows fluid diffusion through the shell wall.

Property Extraction

Representative model fits for a 169 μm capsule and a 61 μm capsule tested in dry compression are shown in Fig. 10. The model was fit to the experimental data using Young's modulus as the single adjustable parameter. Modulus values of the shell wall material were obtained through comparison with the model described above for both dry and immersed compression tests and are summarized in Table 1. The model fits show good agreement until the capsules reach displacement values near 15% (yield point) and then the model deviates significantly from the experimental data. The model predicts a maximum of 3–4% strain in the capsule shell wall at this point. Strains of this magnitude are sufficient to initiate damage in other thermosetting polymers and, as mentioned previously, the yield point may indicate the onset of damage in the shell wall. Dye tests have indicated that there is significant leakage of encapsulant fluid only near 45% deformation, but some diffusion of encapsulant fluid may be occurring. This diffusion would have an effect on the load-displacement behavior of the capsules and is not accounted for in the model. A representative model fit for the compression of a 223 μm immersed capsule, Fig. 10, shows similar behavior to the dry tests. In this case, the model again deviates just prior to 15% deformation.

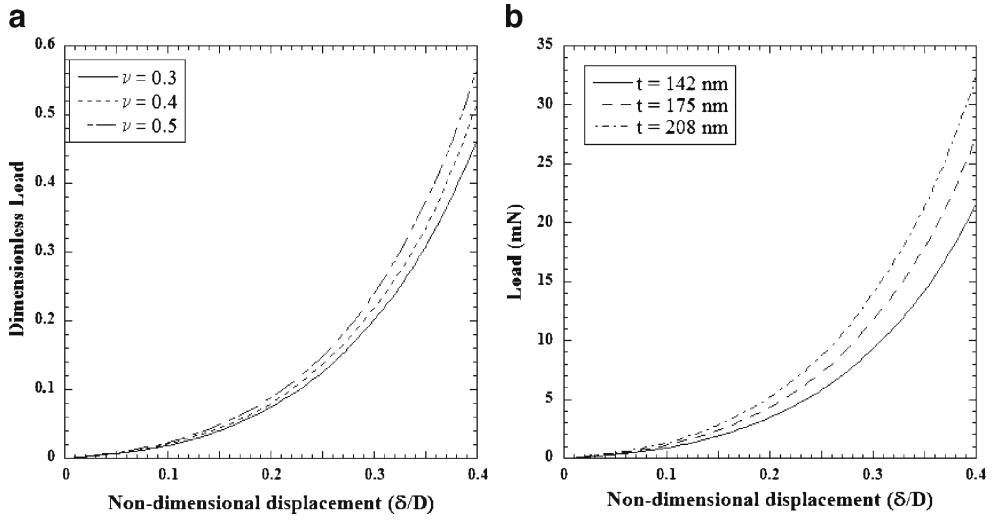

Fig. 9. Load-displacement plots from model parameter studies on the (**a**) effect of Poisson's ratio ($t = 175$ nm) (**b**) effect of shell wall thickness variation for a hypothetical 180 μm capsule with a shell wall modulus of 3.6 GPa

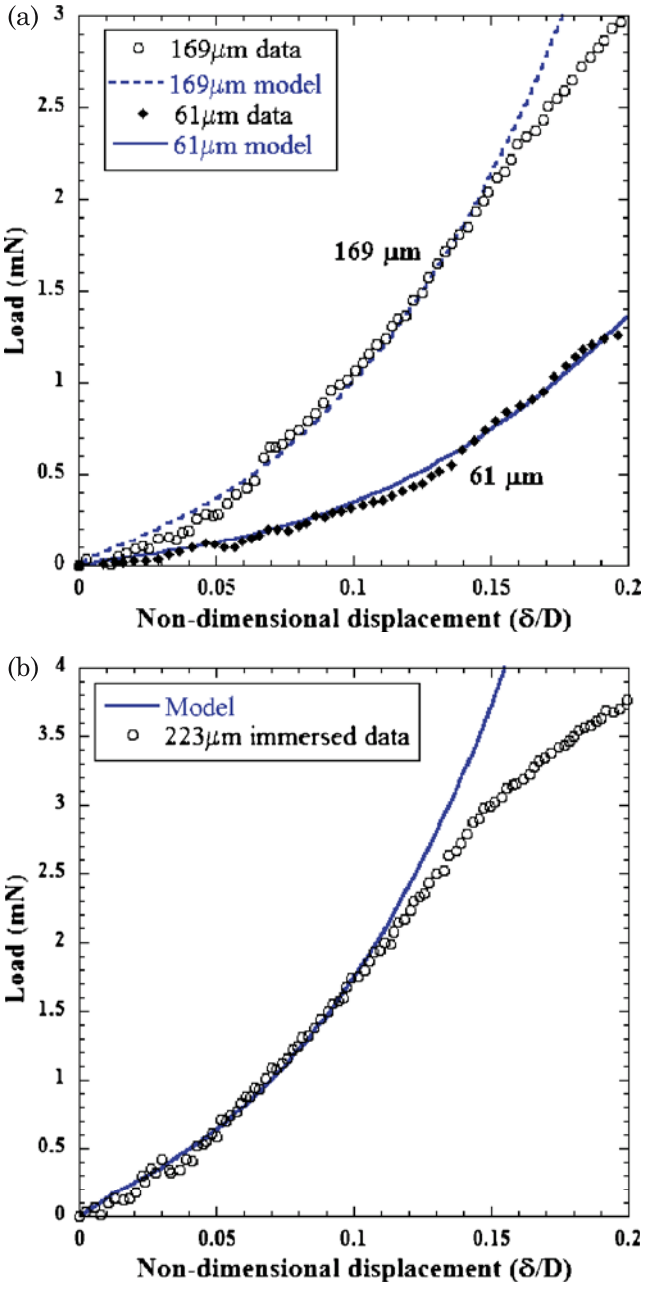

Fig. 10. Comparisons of experimental load-displacement data with the model for (**a**) dry UF capsules and (**b**) immersed UF capsules

Conclusions

The shell wall elastic modulus of poly (urea-formaldehyde) shelled microcapsules was successfully extracted from single capsule compression testing by comparison with a membrane theory model. Young's modulus was found to have an average value of 3.7±0.2 GPa for all capsule testing conditions and was independent of capsule diameter. However, capsule failure behavior was found to be highly diameter dependent. Capsules of smaller diameters, while failing at lower loads, have a higher normalized failure strength.

Acknowledgments The authors would like to acknowledge support from the National Science Foundation (Grant NSF CMS 02-18863) and NASA/JPL (subcontract 1270900). The electron microscopy was performed with the assistance of S. Robinson in the Imaging Technology Group at the Beckman Institute, University of Illinois Urbana-Champaign. The authors would also like to thank Prof. S.R. White and Prof. G. Gioia for fruitful discussions.

References

1. White SR, Sottos NR, Geubelle PH, Moore JS, Kessler MR, Sriram SR, Brown EN, Viswanathan S (2001) Autonomic healing of polymer composites. Nat 409:794–797.
2. Brown EN, White SR, Sottos NR (2002) Fracture testing of a self-healing polymer composite. Exp Mech 42(4):372–379.
3. Brown EN (2003) Fracture and fatigue of a self-healing polymer composite material. PhD thesis, Department of Theoretical and Applied Mechanics, University of Illinois Urbana-Champaign.
4. Brown EN, White SR, Sottos NR (2005) Retardation and repair of fatigue cracks in a microcapsule toughened epoxy composite. Part 1: Manual infiltration. Compos Sci Technol 65(15–16):2466–2473.
5. Brown EN, White SR, Sottos NR (2005) Retardation and repair of fatigue cracks in a microcapsule toughened epoxy composite. Part 2: in-situ healing. Compos Sci Technol 65(15-16):2474–2480.
6. Brown EN, White SR, Sottos NR (2006) Fatigue crack propogation in microcapsule toughened epoxy. J Mat Sci (in press).
7. Brown EN, White SR, Sottos NR (2004) Microcapsule induced toughening in a self-healing polymer composite. J Mat Sci 39:1703–1710.
8. Keller MW, Sottos NR (2004) Effect of microcapsule properties on self-healing composite performance. In: Proceedings of the 2004 SEM X International Congress on Experimental and Applied Mechanics.
9. Mitchison JM, Swan MM (1954) The mechanical properties of the cell surface 1: The cell elastimeter. J Exp Biol 32:443–460.
10. Jay AWL, Edwards MA (1968) Mechanical properties of semipermeable microcapsules. Can J Physiol Pharmacol 46:731–737.
11. Cole KS (1937) Surface forces on an arbacia egg. J Cell Comp Physiol 1:1–9.
12. Liu KK, Williams DR, Briscoe BJ (1996) Compressive deformation of a single microcapsule. Phys Rev E 54(6):6673–6680.
13. Sun G, Zhang Z (2004) Mechanical strength of microcapsules made of different wall materials. Int J Pharm 242:303–307.
14. Zhang Z, Saunders R, Thomas CR (1999) Strength of single microcapsules determined by a novel micromanipulation technique. J Microencapsul 16:117–124.
15. Lulevich VV, Andrienko D, Vinogradova OI (2004) Elasticity of polyelectrolyte multilayer microcapsules. J Chem Phys 120:3822–3826.
16. Dubreuil F, Elsner N, Fery A (2003) Elastic properties of polyelectrolyte capsules studied by atomic-force microscopy and ricm. Eur Phys J E 12:215–221.

17. Gordon VD, Chen X, Hutchinson JW, Bausch AR, Marquez M, Weitz DA (2004) Self-assembled polymer membrane capsules inflated by osmotic pressure. J Am Chem Soc 126: 14117–14122.
18. Hsu MF, Nikolaides MG, Dinsmore AD, Bausch AR, Gordon VD, Chen X, Hutchinson JW, Weitz DA (2005) Fabrication and characterization of self-assembled shells composed of poly(styrene) particles. Langmuir 21:2963–2970.
19. Brown EN, Kessler MR, Sottos NR, White SR (2003) In situ poly(urea-formaldehyde) microencapsulation of dicyclopentadiene. J Microencapsul 20(6):719–730.
20. Feng WW, Yang WH (1973) On the contact problem of an inflated spherical nonlinear membrane. J Appl Mech 40: 209–214.
21. Lardner TJ, Pujara P (1980) Compression of spherical cells. In: Nemat-Nassar S (ed) Mechanics Today, Pergamon, New York, pp 161–176.
22. Wang CX, Wang L, Thomas CR (2004) Modeling the mechanical properties of single suspension-cultured tomato cells. Ann Bot 93:443–453.
23. Cheng LY (1987) Deformation analyses in cell and development biologies. Part I: Formal methodology. J Biomed Eng 109:10–17.